Kang, S., et al., 2022, Paleoclimates inform on a weakening and amplitude-reduced East Asian winter monsoon in the warming future: Geology, v. 50, https://doi.org/10.1130/G50246.1

Supplemental Material

Title: Paleoclimates inform on a weakening and amplitude-reduced East Asian winter monsoon in the warming future

Shugang Kang[1,2,3]*, Xulong Wang[1,2,4], Jinhua Du[5] and Yougui Song[1,2]

[1]State Key Laboratory of Loess and Quaternary Geology, Institute of Earth Environment, Chinese Academy of Sciences, Xi'an 710061, China.
[2]Chinese Academy of Sciences Center for Excellence in Quaternary Science and Global Change, Xi'an 710061, China.
[3]National Observation and Research Station of Earth Critical Zone on the Loess Plateau of Shaanxi, Xi'an 710061, China.
[4]Southern Marine Science and Engineering Guangdong Laboratory (Zhuhai), Zhuhai 519082, China.
[5]School of Earth Science and Resources, Chang'an University, Xi'an 710054, China.

*E-mail: kshg@ieecas.cn

Table S1 Quartz (4–11 μm) optically stimulated luminescence (OSL) ages at WN2 and GB and their related parameters. Data shown in bold were obtained in this study, and the remaining data were from previous studies of WN2 (Kang et al., 2018) and GB (Kang et al., 2020). Details of OSL dating were given in previous studies (Kang et al., 2018, 2020).

Section	Sample ID	Depth (cm)	U (ppm)	Th (ppm)	K (%)	Water content (%)	Dose rate (Gy ka^{-1})	Dose (Gy)	Age (ka)
WN2	WN2-10	10	2.38±0.07	12.92±0.39	2.09±0.06	20±5	3.70±0.18	0.79±0.03	0.21±0.01
	WN2-20	**20**	**2.38±0.07**	**13.23±0.40**	**2.15±0.06**	**20±5**	**3.75±0.18**	**1.36±0.06**	**0.36±0.02**
	WN2-30	30	2.37±0.07	12.75±0.38	2.11±0.06	20±5	3.66±0.18	1.82±0.07	0.50±0.03
	WN2-40	**40**	**2.63±0.08**	**14.34±0.43**	**2.11±0.06**	**20±5**	**3.85±0.19**	**1.87±0.08**	**0.48±0.03**
	WN2-50	50	2.61±0.08	13.70±0.41	2.11±0.06	20±5	3.79±0.19	2.14±0.09	0.56±0.04
	WN2-60	**60**	**2.70±0.08**	**14.67±0.44**	**2.20±0.07**	**20±5**	**3.96±0.20**	**2.58±0.11**	**0.65±0.04**
	WN2-70	70	2.63±0.08	14.91±0.45	2.23±0.07	20±5	3.99±0.20	3.54±0.14	0.89±0.06
	WN2-80	**80**	**2.69±0.08**	**14.43±0.43**	**2.16±0.06**	**20±5**	**3.90±0.19**	**4.03±0.16**	**1.03±0.07**
	WN2-90	90	2.76±0.08	14.65±0.44	2.12±0.06	20±5	3.90±0.19	4.47±0.18	1.14±0.07
	WN2-100	**100**	**2.70±0.08**	**14.75±0.44**	**2.21±0.07**	**20±5**	**3.97±0.20**	**5.27±0.21**	**1.33±0.08**
GB	GB-100	100	2.68±0.10	13.11±0.08	1.64±0.05	10±5	3.72±0.14	14.36±0.59	3.86±0.21
	GB-110	110	2.53±0.03	12.56±0.33	1.63±0.03	10±5	3.61±0.13	16.95±0.68	4.70±0.25
	GB-120	120	2.37±0.07	12.47±0.14	1.64±0.02	10±5	3.56±0.13	18.73±0.77	5.27±0.29
	GB-130	130	2.27±0.05	11.94±0.14	1.64±0.05	10±5	3.48±0.13	19.47±0.82	5.60±0.31
	GB-140	140	2.23±0.05	11.96±0.26	1.65±0.03	10±5	3.48±0.13	21.20±0.86	6.10±0.33
	GB-150	150	2.16±0.01	11.39±0.13	1.59±0.06	10±5	3.35±0.13	23.23±0.93	6.94±0.38
	GB-160	160	2.20±0.06	12.16±0.20	1.65±0.03	10±5	3.48±0.13	24.26±0.99	6.97±0.38
	GB-170	170	2.57±0.03	13.20±0.19	1.70±0.02	10±5	3.73±0.13	26.17±1.05	7.02±0.38
	GB-180	180	2.40±0.00	12.51±0.07	1.63±0.07	10±5	3.55±0.13	29.89±1.21	8.41±0.46
	GB-190	190	2.30±0.03	11.91±0.08	1.61±0.06	10±5	3.45±0.13	32.49±1.31	9.43±0.52
	GB-200	200	2.09±0.04	10.47±0.14	1.58±0.05	10±5	3.23±0.12	33.34±1.34	10.34±0.57
	GB-220	220	2.08±0.05	11.15±0.22	1.59±0.01	10±5	3.28±0.12	36.16±1.45	11.02±0.59
	GB-240	240	1.91±0.11	10.09±0.36	1.56±0.05	10±5	3.11±0.12	39.16±1.57	12.60±0.70
	GB-260	**260**	**1.94±0.08**	**10.41±0.47**	**1.59±0.02**	**10±5**	**3.17±0.12**	**38.15±1.54**	**12.05±0.66**
	GB-300	**300**	**2.02±0.03**	**10.45±0.09**	**1.59±0.01**	**10±5**	**3.19±0.11**	**43.56±1.77**	**13.65±0.73**
	GB-340	**340**	**2.14±0.02**	**11.18±0.29**	**1.62±0.03**	**10±5**	**3.32±0.12**	**47.73±2.02**	**14.40±0.80**
	GB-380	**380**	**2.03±0.07**	**10.39±0.05**	**1.67±0.02**	**10±5**	**3.25±0.12**	**49.39±2.06**	**15.18±0.84**
	GB-420	**420**	**2.05±0.08**	**10.83±0.08**	**1.63±0.01**	**10±5**	**3.25±0.12**	**58.31±2.40**	**17.94±0.98**
	GB-460	**460**	**2.17±0.08**	**10.70±0.19**	**1.63±0.03**	**10±5**	**3.27±0.12**	**56.78±2.30**	**17.39±0.95**
	GB-500	**500**	**2.24±0.04**	**1075±0.12**	**1.80±0.02**	**10±5**	**3.45±0.13**	**56.58±2.28**	**16.42±0.89**
	GB-520	**520**	**2.34±0.03**	**11.38±0.08**	**1.88±0.01**	**10±5**	**3.61±0.13**	**61.82±2.51**	**17.12±0.93**
	GB-540	**540**	**2.37±0.05**	**11.04±0.13**	**1.82±0.03**	**10±5**	**3.53±0.13**	**65.98±2.73**	**18.71±1.03**
	GB-600	**600**	**2.35±0.02**	**10.82±0.11**	**1.91±0.02**	**10±5**	**3.58±0.13**	**66.57±2.85**	**18.59±1.04**
	GB-660	**660**	**2.29±0.02**	**10.64±0.10**	**1.77±0.03**	**10±5**	**3.41±0.13**	**62.93±3.33**	**18.46±1.19**
	GB-720	**720**	**2.35±0.04**	**11.05±0.18**	**1.93±0.01**	**10±5**	**3.60±0.13**	**68.16±2.79**	**18.92±1.04**
	GB-780	**780**	**2.15±0.03**	**10.13±0.06**	**1.76±0.02**	**10±5**	**3.30±0.12**	**67.69±2.92**	**20.51±1.16**
	GB-840	**840**	**2.50±0.03**	**11.13±0.09**	**1.91±0.02**	**10±5**	**3.64±0.13**	**70.90±2.89**	**19.51±1.07**
	GB-860	**860**	**2.35±0.04**	**11.10±0.05**	**1.80±0.01**	**10±5**	**3.48±0.13**	**70.63±2.91**	**20.31±1.11**
	GB-900	**900**	**2.30±0.02**	**10.77±0.09**	**1.87±0.01**	**10±5**	**3.49±0.13**	**72.67±2.98**	**20.80±1.14**
	GB-980	**980**	**2.35±0.03**	**10.71±0.08**	**1.88±0.06**	**10±5**	**3.51±0.13**	**79.58±3.25**	**22.70±1.27**
	GB-1060	**1060**	**2.45±0.02**	**11.12±0.06**	**1.88±0.06**	**10±5**	**3.57±0.14**	**76.23±3.21**	**21.35±1.22**
	GB-1140	**1140**	**2.36±0.02**	**11.08±0.17**	**1.82±0.03**	**10±5**	**3.48±0.13**	**76.86±3.16**	**22.09±1.22**
	GB-1220	**1220**	**2.32±0.03**	**11.29±0.08**	**1.84±0.03**	**10±5**	**3.51±0.13**	**79.30±3.40**	**22.62±1.28**
	GB-1300	**1300**	**2.40±0.04**	**11.39±0.13**	**1.78±0.02**	**10±5**	**3.48±0.13**	**81.68±3.32**	**23.49±1.29**
	GB-1400	**1400**	**2.33±0.04**	**10.53±0.06**	**1.83±0.05**	**10±5**	**3.42±0.13**	**81.37±3.29**	**23.79±1.32**
	GB-1500	**1500**	**2.35±0.03**	**11.11±0.09**	**1.87±0.01**	**10±5**	**3.51±0.13**	**87.27±3.58**	**24.85±1.36**
	GB-1600	**1600**	**2.35±0.04**	**10.79±0.20**	**1.83±0.03**	**10±5**	**3.45±0.13**	**84.43±3.46**	**24.50±1.36**
	GB-1700	**1700**	**2.35±0.02**	**10.84±0.15**	**1.88±0.02**	**10±5**	**3.49±0.13**	**90.00±3.86**	**25.79±1.46**
	GB-1800	**1800**	**2.41±0.03**	**11.37±0.08**	**1.85±0.02**	**10±5**	**3.52±0.13**	**91.46±3.82**	**25.97±1.44**
	GB-1900	**1900**	**2.33±0.03**	**11.11±0.13**	**1.84±0.02**	**10±5**	**3.46±0.13**	**97.10±3.91**	**28.05±1.53**

Table S2 Mean time resolution during specific periods in loess sections GL, JY, GB, and WN2. The resolutions were calculated according to the chronology in Fig. 2 and determined by the proxy sample interval and the times covering specific periods.

Section	Period (ka BP)	Mean resolution (ka)	Reference
GL	~700-2	0.08	Sun et al., 2021
	~688-626 (MIS 16)	0.05	
	~626-568 (MIS 15)	0.14	
	~568-510 (MIS 14)	0.11	
	~510-478 (MIS 13)	0.24	
	~478-426 (MIS 12)	0.05	
	~426-395 (MIS 11)	0.18	
	~395-335 (MIS 10)	0.07	
	~335-281 (MIS 9)	0.13	
	~281-242 (MIS 8)	0.05	
	~242-192 (MIS 7)	0.11	
	~192-129 (MIS 6)	0.08	
	~129-77 (MIS 5)	0.10	
	~77-60 (MIS 4)	0.03	
	~60-30 (MIS 3)	0.05	
	~30-11.5 (MIS 2)	0.05	
	~11.5-2 (MIS 1)	0.15	
JY	~30-2	0.04	Sun et al., 2012; this study
	~30-12 (MIS 2)	0.03	
	~12-2 (MIS 1)	0.21	
	~26-18 (LGM)	0.03	
	~18-12 (LD)	0.04	
	~8-4 (HTM)	0.31	
GB	~28-4	0.03	Kang et al., 2020, this study
	~28-12 (MIS 2)	0.02	
	~12-4 (MIS 1)	0.11	
	~26-18 (LGM)	0.02	
	~18-12 (LD)	0.04	
	~8-4 (HTM)	0.10	
WN2	~1.22-0.16	0.02	Kang et al., 2018, this study
	~1.11-0.58 (MWP)	0.03	
	~0.56-0.16 (LIA)	0.02	

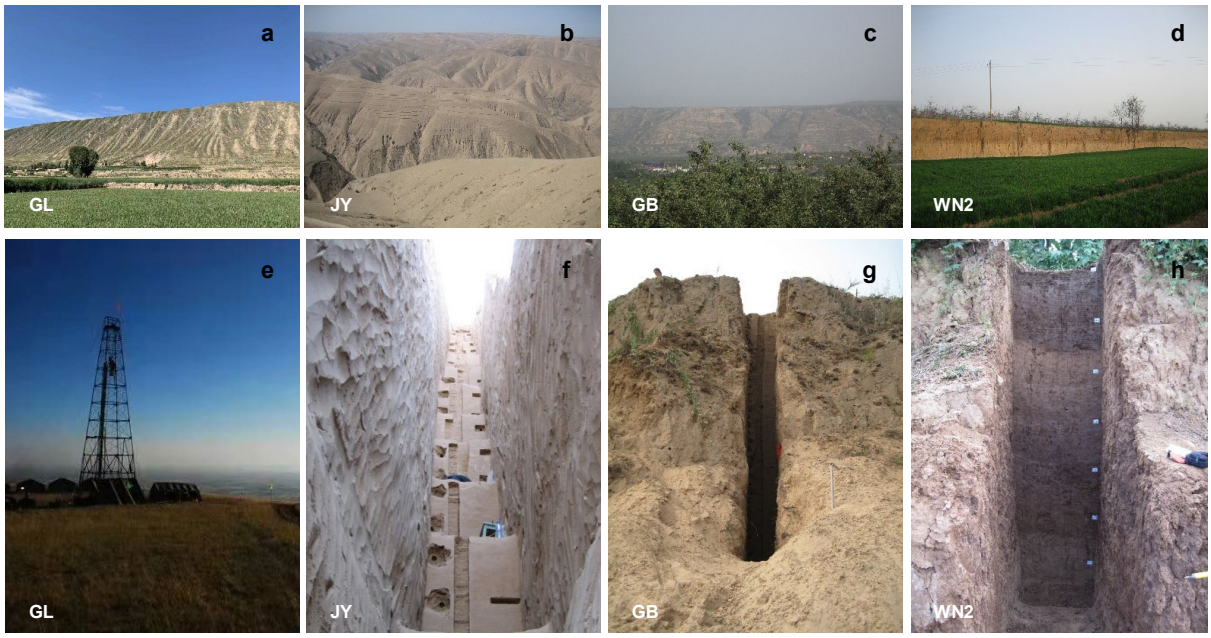

Fig. S1 Loess sedimentation geomorphology, outcrops, sampling pits, and drill cores in the studied sections. Core drilling was conducted at GL (Sun et al., 2021), and sampling pits were excavated at JY (Sun et al., 2012), GB (Kang et al., 2020; this study), and WN2 (Kang et al., 2018; this study). Section coordinate and elevation information: GL (37°29'24"N, 102°52'48"E, 2400 m a.s.l.); JY (36°21'N, 104°36'E, 2210 m a.s.l.), WN2 (34°24'54.85"N, 109°33'44.18"E, 646 m a.s.l.), and GB (34°35'2.14"N, 110°36'24.14"E, 470 m a.s.l.).

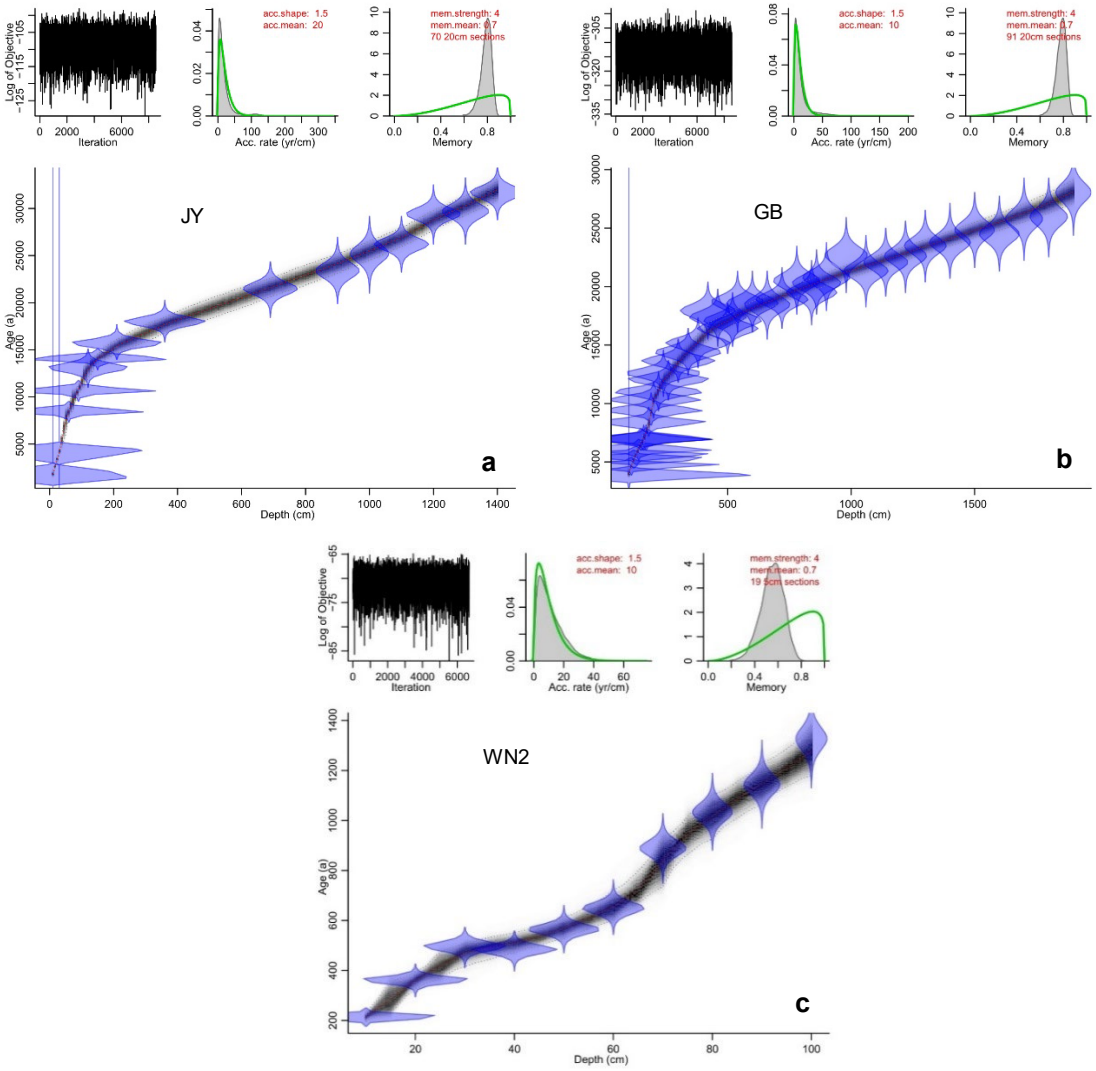

Fig. S2 Output graphs from the Bayesian age-depth model in Bacon software (Blaauw and Christen, 2011) for sections JY (a, Sun et al., 2012; this study), GB (b, Kang et al., 2020; this study), and WN2 (c, Kang et al., 2018; this study). In each subfigure, the upper panel depicts Markov Chain Monte Carlo iterations, prior (green curves) and posterior (gray histograms) distributions for the accumulation rate and memory, and the bottom panel shows OSL ages (transparent blue) and the age-depth model (the darker gray indicates more likely ages; gray dotted lines indicate 95% confidence intervals; red dashed curve shows the 'best' model based on the weighted mean age of each depth).

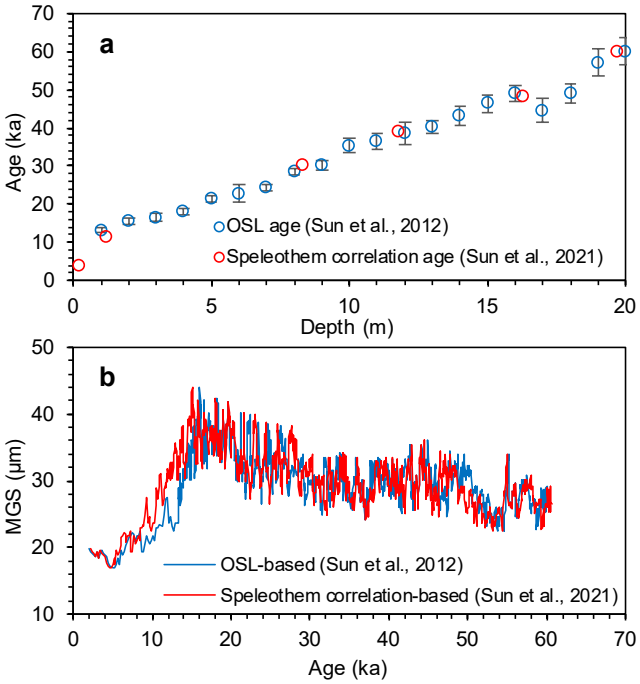

Fig. S3 Comparison of age (a) and mean grain size (b) based on OSL dating (Sun et al., 2012) and speleothem correlation (Sun et al., 2021).

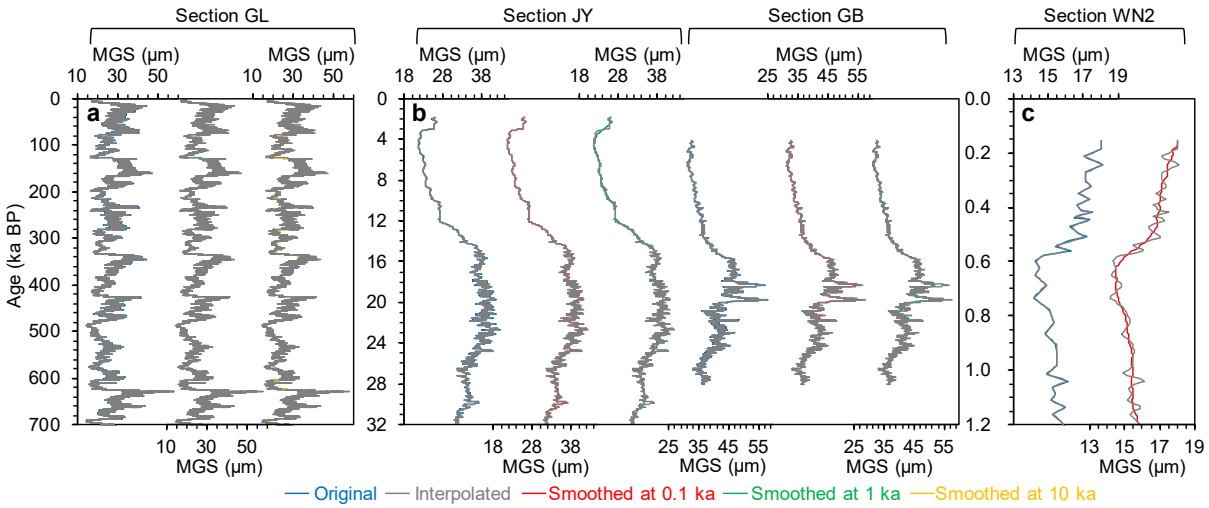

Fig. S4 Linearly interpolated MGS and its smoothing using an adjacent-averaging approach at various time windows (0.1, 1, and 10 ka) at GL (Sun et al., 2021), JY (Sun et al., 2012; this study), GB (Kang et al., 2020; this study), and WN2 (Kang et al., 2018; this study). The interpolation time resolutions are 0.025, 0.02, 0.01, and 0.007 ka at sections GL, JY, GB, and WN2 respectively, which are determined according to corresponding minimum resolution calculated from the constructed chronologies in Fig. 2.

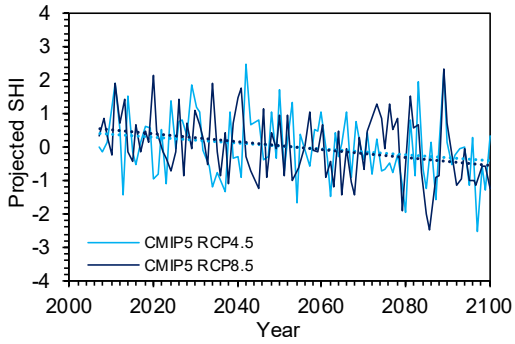

Fig. S5 CMIP5-projected Siberian High index (SHI) during 2007–2100 under RCP4.5 (light blue solid line) and PCP8.5 (blue solid line) scenarios (Li and Gao, 2015). The dashed lines indicate corresponding long-term variation trends.

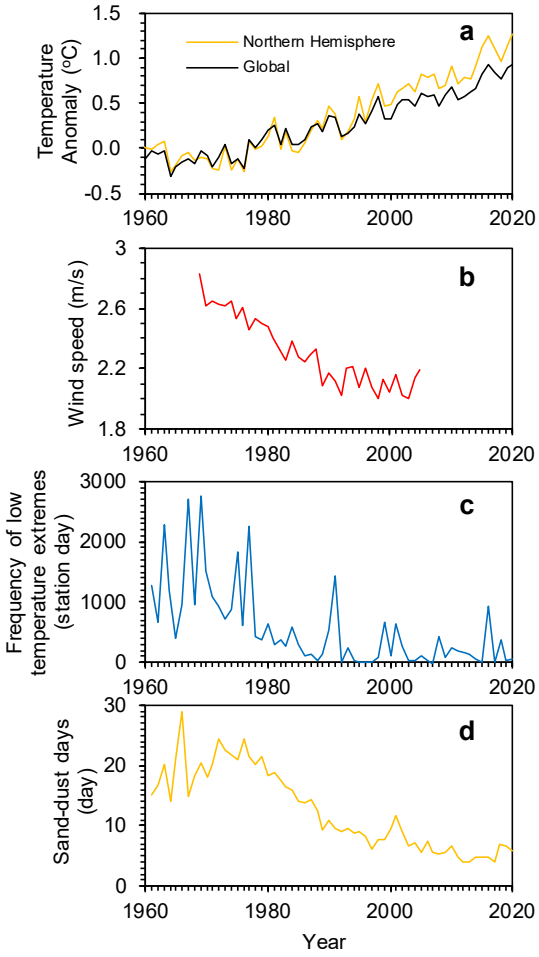

Fig. S6 Variations in winter wind speed, low temperature extremes, and dust storms in China during 1960–2020. a Global and Northern Hemisphere annual surface temperature anomaly relative to 1961–1990 (Morice et al., 2021).**b** Winter wind speed in China during 1969–2005 (Guo et al., 2011). **c** Frequency of annual low temperature extremes in China during 1960–2020 (CMA Climate Change Centre, 2021). **d** Annual sand-dust days during 1960–2020 in China (CMA Climate Change Centre, 2021).

REFERENCES CITED

Blaauw, M., and Christen, J.A., 2011, Flexible Paleoclimate Age-Depth Models Using an Autoregressive Gamma Process: Bayesian Analysis, v. 6, no. 3, p. 457-474, https://doi.org/10.1214/ba/1339616472.

CMA (China Meteorological Administration) Climate Change Centre, 2021, Blue Book on Climate Change in China (2021), Beijing, Science Press, 109 p.

Guo, H., Xu, M., and Hu, Q., 2011, Changes in near-surface wind speed in China: 1969–2005: International Journal of Climatology, v. 31, no. 3, p. 349-358, https://doi.org/10.1002/joc.2091.

Kang, S., Du, J., Wang, N., Dong, J., Wang, D., Wang, X., Qiang, X., and Song, Y., 2020, Early Holocene weakening and mid- to late Holocene strengthening of the East Asian winter monsoon: Geology, v. 48, no. 11, p. 1043-1047, https://doi.org/10.1130/G47621.1.

Kang, S., Wang, X., Roberts, H. M., Duller, G. A. T., Cheng, P., Lu, Y., and An, Z., 2018, Late Holocene anti-phase change in the East Asian summer and winter monsoons: Quaternary Science Reviews, v. 188, p. 28-36, https://doi.org/10.1016/j.quascirev.2018.03.028.

Li, F., and Gao, Y.Q., 2015, The Project Siberian High in CMIP5 Models: Atmospheric and Oceanic Science Letters, v. 8, no. 4, p. 179-184, https://doi.org/10.3878/AOSL20140101.

Morice, C. P., Kennedy, J. J., Rayner, N. A., Winn, J. P., Hogan, E., Killick, R. E., Dunn, R. J. H., Osborn, T. J., Jones, P. D., and Simpson, I. R., 2021, An Updated Assessment of Near-Surface Temperature Change From 1850: The HadCRUT5 Data Set: Journal of Geophysical Research: Atmospheres, v. 126, no. 3, p. e2019JD032361, https://doi.org/10.1029/2019JD032361.

Sun, Y., Clemens, S. C., Guo, F., Liu, X., Wang, Y., Yan, Y., and Liang, L., 2021, High-sedimentation-rate loess records: A new window into understanding orbital- and millennial-scale monsoon variability: Earth-Science Reviews, v. 220, p. 103731, https://doi.org/10.1038/ngeo1326.

Sun, Y. B., Clemens, S. C., Morrill, C., Lin, X. P., Wang, X. L., and An, Z. S., 2012, Influence of Atlantic meridional overturning circulation on the East Asian winter monsoon: Nature Geoscience, v. 5, no. 1, p. 46-49, https://doi.org/10.1016/j.earscirev.2021.103731.